Marine Pollution Bulletin 150 (2020) 110681

Contents lists available at ScienceDirect

Marine Pollution Bulletin

journal homepage: www.elsevier.com/locate/marpolbul

Denitrifying anaerobic methane oxidation in marsh sediments of Chongming eastern intertidal flat

Feiyang Chen[a], Yanling Zheng[a,b,c,**], Lijun Hou[a,*], Jie Zhou[a], Guoyu Yin[b,c], Min Liu[b,c]

[a] State Key Laboratory of Estuarine and Coastal Research, East China Normal University, 500 Dongchuan Road, Minhang District, Shanghai, 200241, China
[b] School of Geographic Sciences, East China Normal University, 500 Dongchuan Road, Minhang District, Shanghai, 200241, China
[c] Key Laboratory of Geographic Information Science (Ministry of Education), East China Normal University, 500 Dongchuan Road, Minhang District, Shanghai, 200241, China

ARTICLE INFO

Keywords:
Denitrifying anaerobic methane oxidation (DAMO)
Nitrogen
Intertidal marshes
The yangtze estuary

ABSTRACT

Denitrifying anaerobic methane oxidation (DAMO) and associated microbial diversity and abundance in the marsh sediments of Chongming eastern intertidal flat, the Yangtze Estuary, were investigated using carbon-isotope tracing and molecular techniques. Co-existence of nitrate-DAMO archaea and nitrite-DAMO bacteria was evidenced, with higher biodiversity of DAMO archaea than DAMO bacteria. Abundance of DAMO archaeal *mcrA* gene and DAMO bacterial *pmoA* gene ranged from 4.2×10^3 to 3.9×10^{10} copies g^{-1} and from 4.5×10^5 to 6.4×10^6 copies g^{-1}, respectively. High DAMO potential was detected, ranging from 0.6 to 46.7 nmol $^{13}CO_2$ g^{-1} day^{-1} for nitrate-DAMO and from 1.3 to 39.9 nmol $^{13}CO_2$ g^{-1} day^{-1} for nitrite-DAMO. In addition to playing an important role as a CH_4 sink, DAMO bacteria also removed a substantial amount of reactive nitrogen (29.4 nmol N g^{-1} day^{-1}) from the intertidal sediments. Overall, these results indicate the importance of DAMO bioprocess as methane and nitrate sinks in intertidal marshes.

1. Introduction

Since the beginning of the industrial era, rising populations, intensive agricultural activities, increased deforestation and land use, related energy use from fossil fuel sources and industrialization have all contributed to the increase in atmospheric greenhouse gas levels (Schwietzke et al., 2016). Methane (CH_4), as the second largest greenhouse gas after carbon dioxide (CO_2), is one of the major "contributors" to the global greenhouse effect, and its production and consumption are an important part of the global carbon cycle. Over century time scales, CH_4 is a more potent greenhouse gas than CO_2 (Bastviken et al., 2011). For a time horizon of 100 years, it is approximately 28 times more efficient at trapping heat in the earth's atmosphere compared to CO_2, and the current level of CH_4 in the atmosphere is higher than at any point in the past 2000 years (Myhre et al., 2013). It is estimated that the contribution of CH_4 to global warming is nearly 22% to date (Dean et al., 2018; Myhre et al., 2013; Wang et al., 2019) and will be further increased with the continuous CH_4 accumulation in the atmosphere.

Microbial-mediated CH_4 production and consumption play a pivotal role in regulating global warming. Global annual CH_4 production was estimated at 300 Tg, 60% of which was oxidized by microorganisms (Knittel and Boetius, 2009). Thus, methane-oxidizing microorganisms have an essential role in counteracting biological CH_4 production and its release to the atmosphere. CH_4 has long been thought to be oxidized by microorganisms only under aerobic conditions. The discovery of the sulfate-dependent anaerobic methane oxidation (sulfate-AOM) in anoxic marine environments has altered this conventional understanding (Barnes and Goldberg, 1976). Previous studies have demonstrated that the sulfate-AOM process converted 90% of CH_4 in marine environments (Hinrichs et al., 1999). However, based on the thermodynamics (Table S1), nitrate- and nitrite-DAMO are far more likely to occur than the sulfate-AOM process in the environments where nitrate (NO_3^-)/nitrite (NO_2^-) and sulfate (SO_4^{2-}) coexist (Strous and Jetten, 2004).

The biological process known as denitrifying anaerobic methane oxidation (DAMO) was first confirmed by Raghoebarsing and colleagues in a laboratory enrichment culture (Raghoebarsing et al., 2006). Ettwig et al. (2009, 2010) found that the nitrite dependent-DAMO process (nitrite-DAMO) was performed by "*Candidatus* Methylomirabilis oxyfera" (*M. oxyfera*) bacteria, which are closely related to the

* Corresponding author.
** Corresponding author. Key Laboratory of Geographic Information Science (Ministry of Education), East China Normal University, 500 Dongchuan Road, Minhang District, Shanghai, 200241, China.
E-mail addresses: ylzheng@geo.ecnu.edu.cn (Y. Zheng), ljhou@sklec.ecnu.edu.cn (L. Hou).

https://doi.org/10.1016/j.marpolbul.2019.110681
Received 6 August 2019; Received in revised form 18 October 2019; Accepted 21 October 2019
Available online 04 November 2019
0025-326X/

uncultured NC10 phylum. It was believed that DAMO bacteria initially reduced NO_2^- to NO, and the produced NO was dismutated to N_2 and O_2. Subsequently, 3/4 of the intragenerated O_2 was used to oxidize CH_4, while the remaining 1/4 participated in other metabolic activities (Ettwig et al., 2010; Wu et al., 2011). *Candidatus* Methylomirabilis sinica, a novel species in the NC10 phylum, can also perform the nitrite-DAMO process (Shen et al., 2016). In recent years, *M. oxyfera*-like DAMO bacteria has been widely detected in wastewater treatment plants (Xu et al., 2017), lake sediment (Deutzmann and Schink, 2011; Kojima et al., 2012; Wang et al., 2016; Yang et al., 2012), wetlands (Segarra et al., 2015; Shen et al., 2015; Zhang et al., 2018), paddy soil (Shen et al., 2014; Wang et al., 2012; Zhou et al., 2014), and ditch sediments (Luesken et al., 2011a). Furthermore, NO_3^- has been recognized as a crucial electron acceptor in the anaerobic methane oxidation process, and the nitrate-DAMO process was catalyzed by an archaeal lineage belonging to the ANME-2d clade, which is named *Candidatus* Methanoperedens nitroreducens (*M. nitroreducens*) (Haroon et al., 2013). It is capable of using NO_3^- as the final electron acceptor to oxidize CH_4 by the reverse methanogenesis pathway (Haroon et al., 2013). The discovery of the nitrate-DAMO process further verified the biochemical mechanism of denitrifying anaerobic methane oxidation (Zhu et al., 2015).

Coastal wetland is known as a large source of CH_4, emitting 40 to 160 Tg of CH_4 per year, which accounts for 7–30% of global annual CH_4 flux (Segarra et al., 2013). In addition, it is greatly influenced by human activities and suffers from a substantial loading of anthropogenic nitrogen (Kintisch, 2013; Zheng et al., 2016). Therefore, we put forward the hypothesis that coastal wetland is an ideal habitat for the occurrence of DAMO reaction which couples CH_4 oxidation with nitrogen removal processes. In addition, it is also assumed that high DAMO microbial biodiversity may occur in coastal wetlands due to the extensive land-sea interaction. To test these hypotheses, the community composition, diversity, and abundance of DAMO archaea and DAMO bacteria in the marsh sediments of Chongming eastern intertidal flat were investigated based on molecular techniques, and the contributions of DAMO microbes to CH_4 oxidation and nitrogen removal were explored using isotope-tracing methods. The potential links among DAMO archaeal and bacterial abundance, potential DAMO rates, and the environmental variables were also examined. This study provides new insights about the role of DAMO microbes in coastal wetlands.

2. Materials and methods

2.1. Study site and sampling

Sampling sites were located in the Chongming eastern intertidal zone, which is the largest intertidal wetland of the Yangtze Estuary, with a total area of 8500 hm^2. In view of tidal dynamics, the intertidal zone can be divided seawards into three different habitats: the high (H), middle (M), and low (L) intertidal zones (Fig. S1). The high intertidal zone is distinguished by clays, in which the vegetation is dominated by *P. communis*. The sediments of the middle intertidal zone are mainly composed of silts and clays and are dominated by *S. mariqueter*. The low intertidal zone consists of silts mixed with fine sands, and no vegetation develops. Six sediment cores (7.2-cm diameter and 50-cm depth) from the high, middle, and low intertidal zones were collected with PVC corers from a sampling plot (5 × 5 m) in January 2018 (winter) and July 2018 (summer). All sediment cores were transported to the laboratory at 4 °C within 4 h. The sediment cores were sliced every 5 cm, and subsamples from the same layer of the same sampling plot were mixed to form one composite sample. Then, samples from the surface (0–5 cm), middle (15–20 cm), and deep (45–50 cm) layers were selected for further analyses. Samples collected from the high intertidal zone in summer were named SH1 (0–5 cm), SH2 (15–20 cm), and SH3 (45–50 cm). Likewise, samples collected from the middle intertidal zone in summer were named SM1, SM2, and SM3, and from the low intertidal zone in summer were named SL1, SL2, and SL3. In addition, samples from the high, middle, and low intertidal zone in winter were named WH1, WH2, WH3, WM1, WM2, WM3, WL1, WL2, and WL3, respectively. Each sample was divided into two parts: One part for immediate stable isotope tracing experiments and physicochemical analyses, and the other part was stored at −80 °C for molecular experiments.

2.2. Sediment characteristics analysis

Sediment pH and temperature were measured using an IQ150 instrument (IQ Scientific Instruments, USA). Sediment salinity was measured using a salinity meter (Bellingham-Stanley, UK) after sediments were mixed with CO_2-free deionized water (w:v = 1:2.5). Water content was calculated by the weight loss of sediments before and after vacuum freeze-drying (Labconco, USA). Total organic carbon (TOC) was determined by the $K_2Cr_2O_7$ oxidation method. NO_3^-, NO_2^- and ammonium (NH_4^+) were extracted from the sediment with 2 M KCl and evaluated by flow injection analysis (Skalar Analytical SAN + +, Netherlands). Sulfide (H_2S) was determined by an Orion Sure-flow® combination silver-sulfide electrode (Thermo Scientific Orion) as described previously (Hou et al., 2012). SO_4^{2-} was analyzed by an ion chromatograph (Segarra et al., 2013). Ferric iron [Fe(III)] was measured using the phenanthroline method (Tamura et al., 1974). The concentration of CH_4 in pore water was determined via immersing fresh sediments into saturated NaCl solution as described by Winkel et al. (2018). All measurements were conducted in triplicate.

2.3. DAMO potential activity measurements

^{13}C stable isotope was used to measure the potential DAMO activities as previously described (Ettwig et al., 2009; Hu et al., 2014; Shi et al., 2017; Zehnder and Brock, 1979). Briefly, sediments were uniformly mixed with He-purged artificial seawater (with *in situ* salinity) at a ratio (w/v) of 1:3. Approximately 20 ml of slurries were transferred into He-flushed 120-ml glass vials and sealed immediately with an aluminum-silicone rubber pad. To remove the residual oxygen and NO_x^- in the slurries, all the glass vials were preincubated in a constant temperature oscillation incubator (with *in situ* temperature) at 120 rpm in dark for at least 30 h. Subsequently, the vials were divided into three different treatment groups: (a) $^{13}CH_4$ (99.9% ^{13}C); (b) $^{13}CH_4 + NO_2^-$; and (c) $^{13}CH_4 + NO_3^-$. Each treatment was conducted in triplicate. Then, 0.2 ml of He-purged NO_2^- and NO_3^- stock solution was injected into groups (b) and (c), respectively, resulting in a final concentration of 0.5 mM NO_2^- in group (b) and 5 mM NO_3^- in group (c). One ml of $^{13}CH_4$ was injected into vials of groups (a), (b) and (c) resulting in a final concentration of 1% (v/v) in the headspace. Additional sediment slurries without any additions were retained as controls. The incubation was inhibited by injecting 50% $ZnCl_2$ solution after 1 day. The incubation temperatures were 3.5 °C and 31.5 °C for winter and summer samples, respectively. The total yield of CO_2 was determined by gas chromatography (GC-2014, Shimadzu), and the production of $^{13}CO_2$ was analyzed with an isotope ratio mass spectrometer (IRMS, Thermo Fisher Scientific) (Hu et al., 2014; Shen et al., 2017). The potential rates of total DAMO, nitrite-DAMO, and nitrate-DAMO were calculated based on the $^{13}CO_2$ production during the incubation as previously described (Wang et al., 2019).

2.4. DNA extraction, gene amplification and sequencing

The Power Soil DNA kit (MO BIO Laboratories, Carlsbad, CA, USA) was used to extract total DNA from homogenized sediment samples (approximately 0.25 wet weight) according to the manufacturer's instructions. The sediment DNA concentration and quality were determined using a NanoDrop 2000 spectrophotometer (Thermo Fisher Scientific, Waltham, MA, USA). The DAMO archaeal alpha subunit of

the methyl-coenzyme M reductase gene (*mcrA*) was amplified with primers McrA169F/McrA1360R, which resulted in a final 1191 bp PCR product (Vaksmaa et al., 2017a). The DAMO bacterial alpha subunit of the particulate methane monooxygenase gene (*pmoA*) was amplified using a nested PCR approach, consisting of an initial PCR amplification with primers A189_b/cmo682 followed by a second PCR with primers cmo182/cmo568, and the final PCR product was 389 bp (Luesken et al., 2011b). At each sampling site, DNA from different sediment depth was mixed to form one composite sample for PCR amplification and clone library construction. The PCR results were examined via 1% agarose gel electrophoresis and purified by Gel Advance-Gel Extraction system (Viogene). The purified PCR products were then cloned using the T1 vector (TransGen BiotechCo., Ltd, Beijing, China). For each sediment sample, approximately 100 white spot clones were randomly picked and subjected to sequencing. The unique DAMO archaeal *mcrA* sequences and DAMO bacterial *pmoA* sequences obtained in the present study have been deposited in GenBank with accession numbers of MK888344-MK888681 and MK888209-MK888343, respectively.

2.5. Phylogenetic analysis of mcrA and pmoA genes

The qualified sequences with more than 97.0% identities were grouped into operational taxonomic units (OTUs) using the Mothur software (Schloss et al., 2009). The Shannon index, Chao1 richness estimator, and rarefaction curves were also generated with Mothur. Phylogenetic analyses of DAMO archaeal *mcrA* and DAMO bacterial *pmoA* genes were carried out with MEGA 7.0 software using the neighbor-joining method (Kumar et al., 2016). A bootstrap test with 1000 replicates was carried out to test the confidence levels of the phylogenetic tree.

2.6. Quantitative PCR assay

The gene copy numbers of DAMO archaeal *mcrA* and DAMO bacterial *pmoA* were determined using the 7500 real-time PCR system (Applied Biosystems, Canada) and the SYBR Green qPCR method (Costello et al., 1999; Hales et al., 1996; Holmes et al., 1999; Xu et al., 2014). More detailed information for the primers (McrA159F/McrA345R for *mcrA* gene and cmo182/cmo568 for *pmoA* gene) and qPCR protocols used in the study is given in Supplementary Table S2. All reactions were performed in 8-strip thin-well PCR tubes with ultraclean cap strips (ABgene, UK). The qPCR results were determined by 1% agarose gel electrophoresis. The standard curves were constructed according to the serial 10-dilution of the constructed plasmid DNA. Negative controls without template DNA were also run under the same conditions to detect and ensure no exogenous contamination in all experiments. All environmental samples and standard plasmid samples in qPCR were conducted in triplicate.

2.7. Statistical analysis

Coverage of the constructed clone libraries was estimated by the percentage of OTU numbers divided by Chao1 estimator. Pearson correlation analyses were conducted to reveal the links of DAMO microbial abundance and activity with sediment properties using SPSS (Statistical Package for the Social Sciences) version 19.0 (SPSS Inc., Chicago, IL, USA). Correlations of the DAMO archaeal and bacterial community structures with environmental parameters were explored via linear-model-based redundancy analysis (RDA, maximum gradient length was shorter than 4SD) using Canoco software (version 4.5). In this study, the statistical results were considered significant when $P < 0.05$ for all analyses.

3. Results

3.1. Sediment characteristics

The physicochemical features of the sediment samples are shown in Supplementary Table S3. The average temperatures were 3.5 °C and 31.5 °C in winter and summer, respectively. Sediment pH varied from 7.99 to 8.65 and from 7.85 to 8.30 in winter and summer, respectively, with relatively higher pH values in the surface layer (0–5 cm) of the intertidal marsh sediment. Sediment salinity was higher in winter (0.7–2.8) than in summer (0.4–1.4), with an increasing trend from the high to low intertidal zones. CH_4 contents in the sediment pore water varied between 3.06 and 55.26 μg L^{-1}, which tended to be higher in the low intertidal flat and in the deeper layers. The contents of total organic carbon (TOC) and NH_4^+ were markedly lower in winter (0.7–9.0 g kg^{-1} and 0.94–14.17 mg kg^{-1}, respectively) than in summer (4.9–12.3 g kg^{-1} and 3.25–63.68 mg kg^{-1}, respectively). Sediment SO_4^{2-} contents varied from 1.3 to 536.2 g kg^{-1}, with relatively higher value in the upper sediment layers. NO_3^- concentrations ranged from 0.12 to 16.80 mg kg^{-1}, which generally deceased with sediment depth and showed an increasing trend from the high to low intertidal flats. NO_2^- had low contents in all sediment samples but showed relatively higher concentrations in summer (0.02–0.97 mg kg^{-1}) than in winter (0.00–0.05 mg kg^{-1}). Fe(III) contents in the sediment ranged between 0.58 and 1.65 mg g^{-1} with no significant spatial and temporal variations. H_2S contents ranged from 1.70 to 10.54 mg kg^{-1}, which tended to be higher in the deeper layers than in the sediment surface.

3.2. Biodiversity and community composition of DAMO archaea

Specific fragments of the DAMO archaeal *mcrA* gene were successfully amplified from the intertidal marsh sediments. In each individual clone library, 7 to 12 OTUs occurred as defined by 3% divergence in nucleotides. Based on the Shannon-Wiener and Simpson indicators, the diversity of DAMO archaea was greater in winter than in summer and showed an increasing trend from the low to high intertidal flats (Tables 1 and S4). In addition, the diversity of DAMO archaea was significantly higher than that of DAMO bacteria ($P < 0.05$) (Table 1). In this study, the coverage of the DAMO archaeal *mcrA* gene clone library ranged from 96% to 100% (Table 1), showing that the sequenced clones well represented the diversity level of DAMO archaea in this region. Phylogenetic analysis revealed that the obtained *mcrA* sequences were grouped into three distinct clusters (Fig. 1). Phylogenetic analysis showed that the sequences of clusters I and II (accounting for 88.7% of the obtained *mcrA* gene clones) were closely related to known DAMO archaea of *M. nitroreducens* (JMIY01000002) and *Candidatus* Methanoperedens sp. (LKCM01000102) with up to 87.6% and 92.8% gene identities, respectively. *McrA* cluster I, containing 55.7% of all the gene sequences, was also closely related to the clones retrieved from paddy soil (KX290035), freshwater sediment (EU495304), marine sediment (KX290029), and river sediment (KX290024) with up to 97.3% gene identity. Most of the sequences in cluster I were retrieved from the high intertidal zone (48.7%) and the middle intertidal zone (44.3%), with 7.0% of the low intertidal zone sequences associated with this cluster. Further, 33.0% of all the *mcrA* sequences were affiliated to cluster II; however, no similar gene sequences from other environments were associated with this cluster. Most of the clones in cluster II (80.1%) were obtained from the low intertidal zone. Only 11.3% of the *mcrA* clones were affiliated with cluster III, which were only distantly related to *M. nitroreducens* (with 76.2% sequence identity) and *Candidatus* Methanoperedens sp. (with 74.0% sequence identity). Nevertheless, they were closely related to *mcrA* clones retrieved from other environments, such as marine sediment (KX581155) and estuarine sediment (EU681937), with up to 92.4% gene identity. *McrA* genes of this cluster were homogeneously distributed in different intertidal zones, which accounted for 10.5%, 7.9%, and 15.6% of the obtained *mcrA*

Table 1
Diversity characteristics of clone libraries of nitrate-DAMO archaea and nitrite-DAMO bacteria in Chongming eastern intertidal sediments.

gene	Sample	No. of clones	OTUs [a]	Chao1[b]	Shannon[c]	1/Simpson[d]	Coverage (%)[e]
pmoA	SL	97	6	6.0	1.45	3.91	100
	WL	82	2	2.0	0.69	2.01	100
	SM	100	4	4.0	0.52	1.34	100
	WH	99	2	2.0	0.69	2.02	100
	SL	94	8	8.0	1.59	3.93	100
	WL	97	9	9.0	1.96	5.91	100
	SM	97	12	12.2	1.85	4.85	98
mcrA	WM	93	7	7.0	1.58	4.39	100
	SH	95	11	11.5	1.97	5.91	96
	WH	91	9	9.0	1.97	6.59	100

[a] OTUs were defined at 3% nucleotide acid divergence.
[b] Nonparametric statistical predictions of total richess of OTUs based on distribution of singletons and doubletons.
[c] Shannon diversity index. A higher number represents more diversity.
[d] Reciprocal of Simpson's diversity index. A higher number represents more diversity.
[e] The coverage of each clone library was estimated by the percentage of observed number of OTUs divided by Chao1 estimator.

clones in the low, middle, and high intertidal zones, respectively.

3.3. Biodiversity and community composition of the DAMO bacteria

A specific fragment of the DAMO bacterial *pmoA* gene was successfully amplified with nested PCR from the intertidal marsh sediments except for WM and SH (Table 1). In each individual *pmoA* gene clone library, 2 to 6 OTUs were obtained based on a threshold of 3% divergence in nucleotides. Based on the Shannon-Wiener and Simpson indicators, the diversity of DAMO bacteria was greater in winter than in summer (Table 1), and the highest diversity of DAMO bacteria was observed in the low intertidal flat in summer (Table 1). The coverage of the *pmoA* gene clone library was 100% (Table 1), indicating that the *pmoA* clones sequenced in this study well represented the diversity of DAMO bacteria in this study area, which was further confirmed by the rarefaction analyses (Fig. S2). Phylogenetic analysis showed that the DAMO bacterial *pmoA* gene sequences were clustered with known DAMO bacteria of *M. oxyfera* and *M. Sinica* with 88.5–95.6% and 84.6–86.9% sequence identity, respectively (Fig. 2). Based on the constructed phylogenetic tree, the obtained *pmoA* sequences were divided into two distinct clusters (Fig. 2). Cluster I contained 209 sequences accounting for 55.3% of the obtained gene sequences. Further, 63.9%, 46.3%, 10.0%, and 100% of clones from the low intertidal flat in summer and winter, the middle intertidal flat in summer, and the

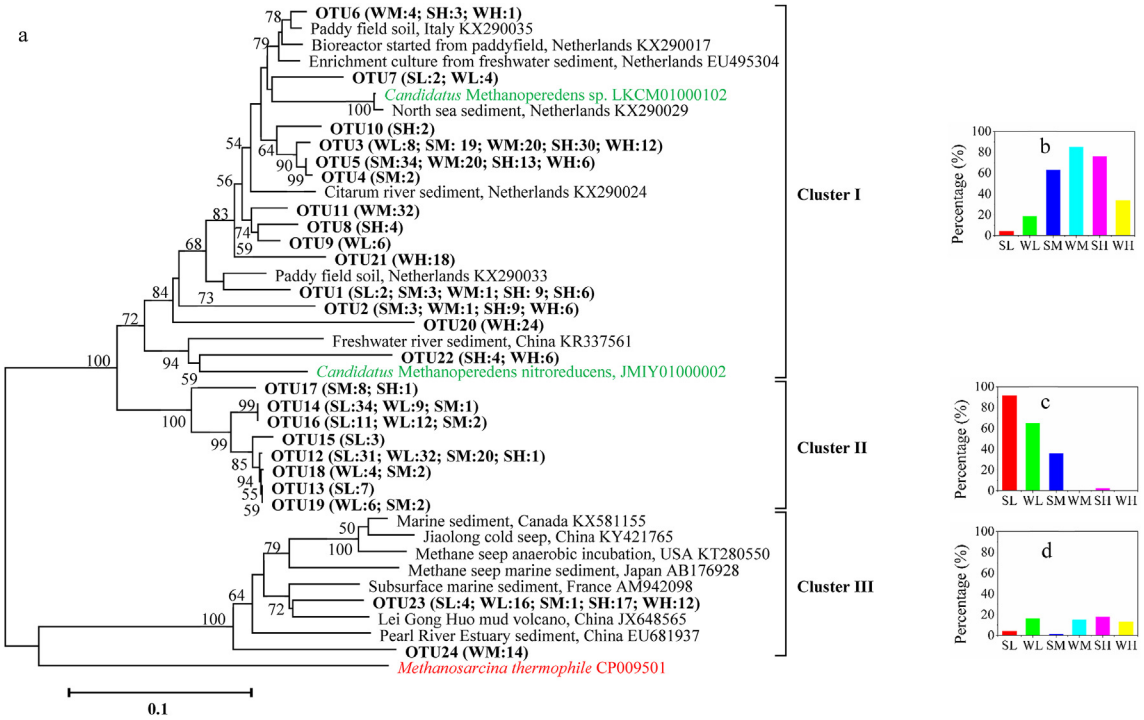

Fig. 1. Neighbor-Joining phylogenetic tree showing the phylogenetic affiliations of nitrate-DAMO archaeal *mcrA* gene sequences recovered from Chongming eastern intertidal marsh sediments (a), and the percentages of sequences in each sample fall into cluster I (b), cluster II (c), and cluster III (d), respectively. The bootstrap valves > 50% (1000 replicates) are shown at the branch nodes. The scale indicates the number of nucleotide substitutions per site. GenBank accession numbers are shown for sequences from other studies. Numbers in parentheses followed each OTU (in bold) indicate the number of sequences recovered from each sampling site. S and W represent summer and winter, respectively. L, M, and H represent the low, middle, and high tidal flats, respectively. Known nitrate-DAMO archaea are shown in green. *Methanosarcina thermophile* (in red) is used as the out-group. Evolutionary analyses were conducted in MEGA7. (For interpretation of the references to colour in this figure legend, the reader is referred to the Web version of this article.)

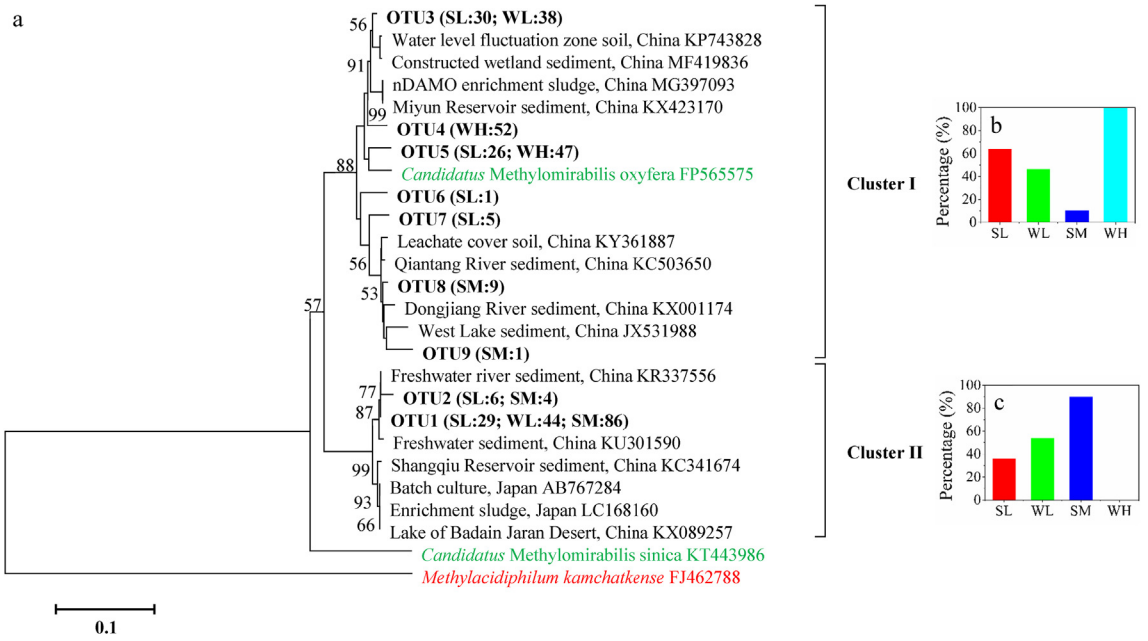

Fig. 2. Neighbor-Joining phylogenetic tree showing the phylogenetic affiliations of nitrite-DAMO bacterial *pmoA* gene sequences recovered from Chongming eastern intertidal marsh sediments (a), and the percentages of sequences in each sample fall into cluster I (b) and cluster II (c) respectively. The bootstrap valves > 50% (1000 replicates) are shown at the branch nodes. The scale indicates the number of nucleotide substitutions per site. GenBank accession numbers are shown for sequences from other studies. Numbers in parentheses followed each OTU (in bold) indicate the number of sequences recovered from each sampling site. S and W represent summer and winter, respectively. L, M, and H represent the low, middle, and high tidal flats, respectively. Known nitrite-DAMO bacteria are shown in green. *Methylacidiphilum kamchatkense* (in red) is used as the out-group. Evolutionary analyses were conducted in MEGA7. (For interpretation of the references to colour in this figure legend, the reader is referred to the Web version of this article.)

high intertidal flat in winter, respectively, were affiliated with this cluster and had 92.1–95.6% gene identity with *M. oxyfera*. These clones also showed high gene identity (up to 98.9%) with *pmoA* sequences retrieved from a water level fluctuation zone (KP743828), a constructed wetland (MF419836), enrichment sludge (MG397093), reservoir sediment (KX423170), river sediment (KC503650), and lake sediment (JX531988). Cluster II contained 169 sequences accounting for 44.7% of the whole gene sequences, all of which were recovered from the middle intertidal zone (53.3%) and the low intertidal zone (46.8%). This cluster showed relatively lower identity (84.6–86.9%) with *M. oxyfera* than cluster I, but was closely related to the *pmoA* clones retrieved from freshwater sediment (KR337556; KU301590) with up to 99.7% gene identity.

3.4. Quantitative analysis of DAMO archaea and DAMO bacteria

In this study, qPCR results showed that the abundances of the DAMO archaeal *mcrA* gene and the DAMO bacterial *pmoA* gene varied from 4.2×10^3 to 3.9×10^{10} copies g^{-1} and from 4.5×10^5 to 6.4×10^6 copies g^{-1} (Fig. 3), respectively. The ratio of the abundance of DAMO archaea to that of DAMO bacteria varied from 9.7×10^{-4} to 7.7×10^3. The average abundance of DAMO archaea was higher in summer (4.3×10^9 copies g^{-1}) than in winter (5.1×10^8 copies g^{-1}), while the average abundance of DAMO bacteria in summer (3.2×10^3 copies g^{-1}) was approximate to that in winter (3.3×10^3 copies g^{-1}). Both the average abundance of DAMO archaea and DAMO bacteria tended to be higher in the low intertidal flat than in the middle and high intertidal zones (Fig. 3). The average abundance of DAMO archaea tended to be higher in the middle sediment layer (15–20 cm), compared with the surface (0–5 cm) and deep (45–50 cm) sediment layers. The abundance of DAMO bacteria showed an increasing trend from the surface layer down to 45–50 cm sediment depth in the low intertidal flat. In contrast, in the middle and high intertidal flats, the abundance of DAMO bacteria decreased with sediment depth.

3.5. Potential methane oxidation rates

The potential anaerobic methane oxidation rates were determined by the ^{13}C stable isotope tracing method. The results revealed that nitrite-DAMO and nitrate-DAMO potentials in the intertidal marsh sediments ranged from 1.3 to 39.9 nmol $^{13}CO_2$ g^{-1} day^{-1} and from 0.6 to 46.7 nmol $^{13}CO_2$ g^{-1} day^{-1}, respectively (Figs. 4 and 5). In summer, the average nitrate-DAMO activity was higher in the low intertidal zone (40.7 nmol $^{13}CO_2$ g^{-1} day^{-1}) and was always higher at the surface layer (0–5 cm) (Fig. 4). In winter, the potential nitrate-DAMO activity increased gradually seawards (from 1.5 to 6.9 nmol $^{13}CO_2$ g^{-1} day^{-1}) and tended to be higher at the middle and deep sediment layers. The average nitrite-DAMO activity showed an increasing trend from the low to high intertidal flats in summer, while the opposite trend was observed in winter. Moreover, the potential nitrite-DAMO rate decreased gradually seawards at different sediment depths, and peaked at the deep layer (45–50 cm). The total DAMO activity in the intertidal marsh sediments was significantly higher in summer (an average rate of 40.5 nmol $^{13}CO_2$ g^{-1} day^{-1}) than in winter (an average rate of 8.2 nmol $^{13}CO_2$ g^{-1} day^{-1}) ($P < 0.05$) (Fig. 4). The ratio of nitrate-DAMO to nitrite-DAMO activity ranged from 0.05 to 33.30 (0.28–2.27 in winter and 0.05–33.30 in summer) (Table S5). Overall, the nitrate-DAMO activity accounted for a higher proportion of total DAMO activity than nitrite-DAMO activity at most sampling sites (Table S5). Furthermore, it was estimated that the nitrogen removal rates ranged between 3.3 and 106.4 nmol N g^{-1} day^{-1} in the intertidal marsh sediments, based on the stoichiometric-relationship of CH_4 and NO_2^- in the DAMO reaction (3:8) (Fig. 5).

3.6. Effects of environmental characteristics on DAMO archaea and DAMO bacteria

The correlations between the DAMO archaeal *mcrA* community composition and environmental factors were explored via RDA (Fig. 6a). The environmental parameters in the first two RDA

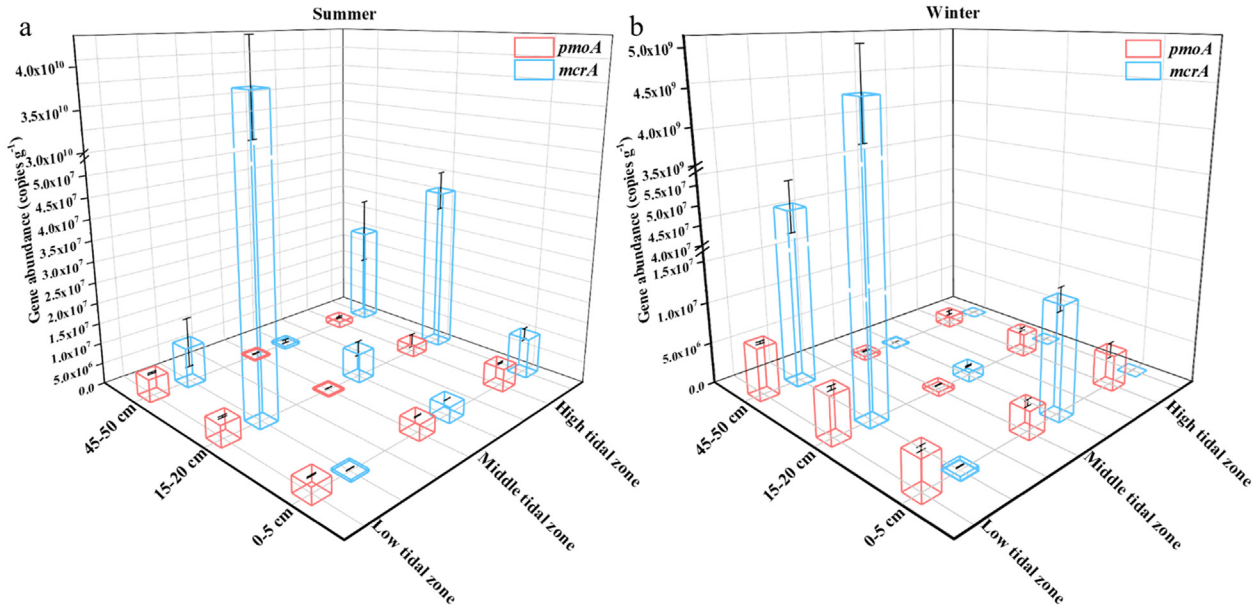

Fig. 3. Abundance of DAMO archaeal *mcrA* gene and DAMO bacterial *pmoA* gene at different intertidal zones and soil depths in summer (a) and winter (b).

dimensions explained 71.5% of the cumulative variance of the genotype-environment relationship. Among the measured environmental variables, only sediment water content contributed significantly ($P = 0.044$, $F = 2.33$, 499 Monte Carlo permutations) to the DAMO archaeal *mcrA*-environment relationship. This factor alone provided 37.0% of the total RDA explanatory power. The relationships between the DAMO bacterial *pmoA* assemblages and environmental variables were also analyzed (Fig. 6b). The first two RDA dimensions explained 97.2% of the cumulative variance of the DAMO bacterial *pmoA*-environment relationship. However, none of the measured environmental characteristics contributed significantly to this relationship ($P > 0.05$). Nitrate-DAMO potential was significantly correlated with temperature, pH, TOC, NO_2^-, H_2S, and Fe(III) ($P < 0.05$), while nitrite-DAMO rate was positively related to temperature and sediment NH_4^+ content ($P < 0.05$) (Table 2). In addition, the significant correlations were found between the total DAMO potential and temperature, pH, TOC, and NH_4^+. The abundance of the DAMO archaeal *mcrA* gene was significantly related to sediment TOC, NO_2^-, and H_2S ($P < 0.05$), while the DAMO bacterial *pmoA* gene was significantly correlated with sediment water content, NO_3^-, and Fe(III) ($P < 0.05$).

4. Discussion

In the present study, our hypothesis that high DAMO microbial biodiversity may occur in coastal wetland was confirmed via molecular techniques. Phylogenetic analysis evidenced that diverse DAMO archaea and DAMO bacteria co-occurred and were widely distributed in different intertidal zones. In the study area, 2–6 *pmoA* gene OTUs based on a 3% cut-off or 2–4 *pmoA* gene OTUs based on a 7% cut-off were observed, which was slightly higher than the DAMO bacteria in the sediments of Lake Constance (Deutzmann and Schink, 2011), Lake Biwa (Kojima et al., 2012), Xiazhuhu and Xixi wetlands (Hu et al., 2014), and

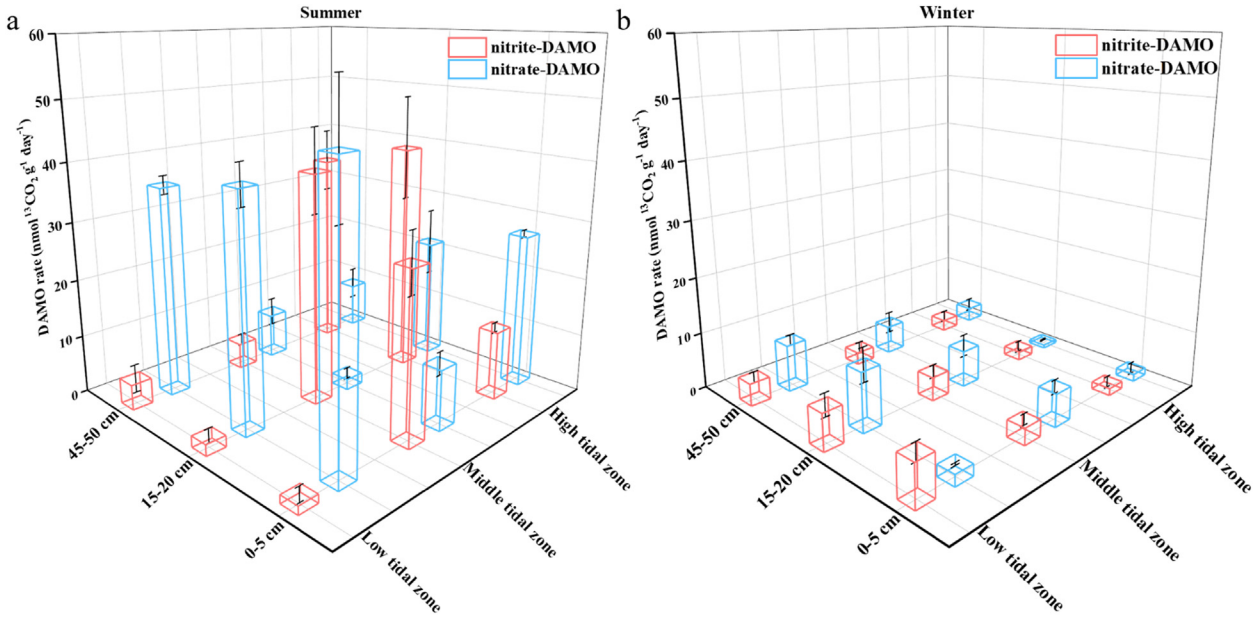

Fig. 4. Potential nitrate-DAMO and nitrite-DAMO activities at different intertidal zones and soil depths in summer (a) and winter (b).

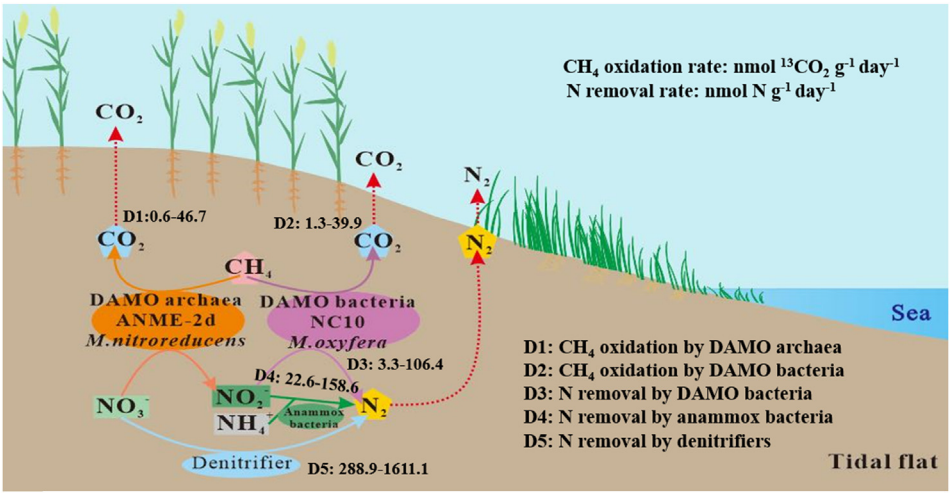

Fig. 5. CH_4 oxidation potentials of DAMO archaea and DAMO bacteria, and nitrogen removal potentials of DAMO bacteria, anammox bacteria, and denitrifiers in intertidal marsh sediments of the Yangtze Estuary.

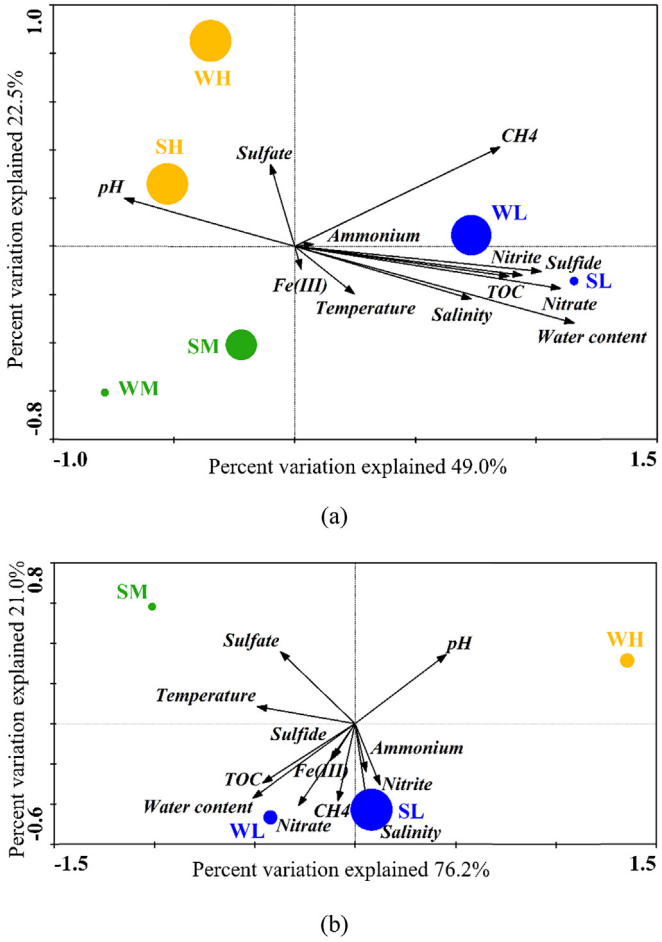

Fig. 6. RDA ordination plots for the first two principal dimensions of the relationship between the DAMO archaeal (a) and DAMO bacterial (b) community compositions with the environmental parameters. The blue circles represent the sampling stations in the low intertidal flat, the green circles represent the sampling stations in the middle intertidal flat, and the yellow circles represent the sampling stations in the high intertidal flat. The size of the circles corresponds to the Shannon' diversity in individual samples. (For interpretation of the references to colour in this figure legend, the reader is referred to the Web version of this article.)

a paddy field (Hu et al., 2014), where only one OTU was observed based on 7% differences. The higher biodiversity of DAMO bacteria observed in the coastal wetland might be attributed to the effect of land-sea interaction, which might bring about different genotypes to this highly dynamic and complex ecosystem. A novel methanotroph species is suggested when the *pmoA* gene nucleic acid sequence identity is lower than 93.0% compared with known species (Lüke and Frenzel, 2011). In the present study, *pmoA* cluster 2 (accounting for 44.7% of all the obtained *pmoA* sequences) was only distantly related (84.6–86.9%) to the *pmoA* gene of *M. oxyfera* (Fig. 2). All sequences in this cluster were recovered from the middle and low intertidal zones, indicating that a potentially novel DAMO bacterial species reduces CH_4 emissions in the *S. mariqueter* and bare mudflat stands. The studies on the occurrence and community dynamics of DAMO archaea in natural environments were quite rare to date. However, the environmental significance of DAMO archaea as well as nitrate-DAMO activity should be investigated, as NO_3^- rather than NO_2^- is the main form of nitrogen oxide caused by human activities in intertidal environments. In this study, the Shannon diversity of DAMO archaea in the intertidal marsh sediments based on the *mcrA* gene (1.58–1.97) was significantly higher than that of DAMO archaea detected in river sediments, paddy soil, and lake sediments based on the 16S rRNA gene (Shannon diversity: 0.12–0.64) (Ding et al., 2015). In addition, the observed DAMO archaeal biodiversity was significantly higher than that of DAMO bacteria in the intertidal marsh sediments ($P < 0.05$) (Table 1). These results suggested that a higher diversity of DAMO archaea might inhabit the intertidal wetland of the Yangtze Estuary.

The functional *mcrA* gene was used to quantify DAMO archaea in the present study, as previous studies showed that the number of DAMO archaea might be overestimated based on 16S rRNA gene primers, which were less specific for DAMO archaea than the *mcrA* gene (Vaksmaa et al., 2017a). The copy number of the DAMO archaeal *mcrA* gene in Chongming eastern intertidal marsh sediments varied from 4.2×10^3 to 3.9×10^{10} copies g^{-1}, which was relatively higher than that detected in paddy soil (7.2×10^3–1.8×10^7 copies g^{-1}) (Vaksmaa et al., 2017a, b), river sediment (3.0×10^4–4.4×10^5 copies g^{-1}) (Vaksmaa et al., 2017a), and marine sediment (2.5×10^4 copies g^{-1}) (Vaksmaa et al., 2017a). The copy number of the DAMO bacterial *pmoA* gene ranged from 4.5×10^5 to 6.4×10^6 copies g^{-1}, which was slightly lower than that in mangrove sediments (2.1×10^6–3.4×10^7 copies g^{-1}) (Zhang et al., 2018) but higher than that in reduced riverbeds (2.4×10^4–8.7×10^4 copies g^{-1}) (Shen et al., 2019). Our data also suggested that there might be an intimate symbiotic relationship between DAMO archaea and bacteria (Wang et al., 2019), as these two

Table 2
Correlation analyses of environmental factors and the activity and abundance of DAMO microbes in Chongming eastern intertidal sediments.

Pearson correlation coefficients	Nitrate-DAMO rate	Nitrite-DAMO rate	Total DAMO rate	DAMO archaeal *mcrA* gene abundance	DAMO bacterial *pmoA* gene abundance
Temperature	**0.599****	**0.575***	**0.874****	0.198	−0.019
pH	**−0.633****	−0.356	**−0.739****	−0.335	−0.431
Salinity	−0.132	−0.463	−0.353	0.041	0.342
Water content	0.458	−0.043	0.314	0.431	**0.591****
TOC	**0.764****	0.308	**0.802****	**0.468***	0.425
NO_3^--N	0.24	−0.299	−0.039	0.299	**0.608****
NO_2^--N	**0.630****	−0.171	0.350	**0.522***	0.366
NH_4^+-N	0.277	**0.480***	**0.561***	0.232	−0.088
Fe(III)	**0.483***	0.03	0.387	0.225	**0.472***
H_2S	**0.590****	0.016	0.457	**0.605****	0.209
SO_4^{2-}	0.058	0.314	0.274	0.05	0.015
CH_4	−0.060	−0.162	−0.164	−0.063	0.457

** and * denote $P < 0.01$ and $P < 0.05$ respectively, which were typically regarded as significant, as determined by SPSS version 19.0 program (SPSS, Chicago, IL). TOC:total organic carbon.

microorganisms co-occurred in the intertidal zone. However, the relative abundance of DAMO bacteria and DAMO archaea varied significantly in different intertidal zones, in particular, with higher abundance of DAMO archaea than DAMO bacteria in the unvegetated low intertidal flat. We speculated that it might be attributed to the different preferences of DAMO bacteria and archaea for oxygen, as DAMO archaea preferred a more anoxic environment (Wang et al., 2019), and some studies showed that a supply of trace oxygen was favorable to DAMO bacteria (Luesken et al., 2011a). The sediment in the low intertidal flat might be more anoxic owing mainly to the more frequent immersion by tidal water and the non-disturbances by the roots of vegetation. It was hypothesized that DAMO archaea can use diverse electron acceptors to anaerobically oxidize CH_4 in addition to NO_3^- (Ettwig et al., 2016). For example, *M. nitroreducens*-like DAMO archaea were reported to oxidize CH_4 using Fe(III) (Ettwig et al., 2016), and it was recently observed that the addition of Fe(III) stimulated expression of the DAMO archaeal *mcrA* gene (Shen et al., 2019). In addition, there is evidence that ANME-2d archaea were involved in sulfate-AOM in lake sediments based on RNA stable isotope probing (RNA-SIP) incubation experiments (Weber et al., 2017). Thus, the high abundance of DAMO archaea in the low intertidal flat might be supported by electron acceptors other than NO_3^-, such as Fe(III) and SO_4^{2-}, although no significant correlation was detected between DAMO archaeal *mcrA* gene abundance and these individual electron acceptors in the present study.

The anaerobic CH_4 oxidation potential of DAMO microorganisms was measured using the ^{13}C stable isotope tracing method. The measured nitrite-DAMO rate in the group amended with $^{13}CH_4 + NO_2^-$ might be higher than that amended with $^{13}CH_4 + NO_3^-$, as NO_2^- for DAMO bacteria in the latter group was provided indirectly. Therefore, it is possible that the potential nitrate-DAMO rate was underestimated in this study, as the indirectly provided NO_2^- was probably not sufficient to support the full CH_4 oxidation capacity of DAMO bacteria. However, the added NO_3^- (5 mM) was sufficient to support the DAMO potential (it remained relatively stable with higher NO_3^- additions), and the produced NO_2^- might be enough for DAMO bacteria to oxidize CH_4. Thus, the possible underestimation of the nitrate-DAMO potential might be not significant here. Given that NO_3^- is typically far more abundant than NO_2^- in intertidal marsh sediments, it is reasonable to use the DAMO rate measured with $^{13}CH_4 + NO_3^-$ to estimate the potential role of both DAMO bacteria and archaea in attenuating CH_4 emissions from intertidal marshes.

The hypothesis that the coastal wetland is an appropriate habitat for the occurrence of DAMO reaction was supported by ^{13}C stable isotope tracing experiments. The potential nitrate-DAMO activity measured in our study varied from 0.6 to 46.7 nmol $^{13}CO_2$ g^{-1} day^{-1}, which was higher than that measured for Zhoushan Island (0–1.57 nmol $^{13}CO_2$ g^{-1} day^{-1}) (Wang et al., 2019). The nitrite-DAMO potential ranged from 1.3 to 39.0 nmol $^{13}CO_2$ g^{-1} day^{-1} in Chongming eastern intertidal marsh sediments, which was approximate to that measured in reduced riverbeds (0.4–61.0 $^{13}CO_2$ g^{-1} day^{-1}) (Shen et al., 2019), but higher than that measured in freshwater wetlands (0.31–5.43 $^{13}CO_2$ g^{-1} day^{-1}) (Hu et al., 2014), paddy fields (1.68–2.04 $^{13}CO_2$ g^{-1} day^{-1}) (Hu et al., 2014), and Zhoushan Island (0–1.51 $^{13}CO_2$ g^{-1} day^{-1}) (Wang et al., 2019). However, even higher nitrite-DAMO rates were reported in mangrove sediments (25.9–704.1 $^{13}CO_2$ g^{-1} day^{-1}) (Zhang et al., 2018). The DAMO potential in summer was significantly higher than that in winter ($P < 0.05$), showing that high temperature might effectively promote the growth and activity of DAMO bacteria and DAMO archaea. In fact, a significant correlation was detected between the potential DAMO rate and temperature ($P < 0.05$) (Table 2). Furthermore, the potential DAMO activity in the low and middle intertidal flat was generally higher than that in the high intertidal flat, where the NO_x^- content also tended to be higher (Fig. 4). However, no significant correlation was observed between them ($P > 0.05$). The ratio of nitrate-DAMO activity to nitrite-DAMO activity ranged from 0.05 to 33.30 (Table S5) with the highest value occurring in the low intertidal flat, further suggesting that the anaerobic sediments in the low intertidal zone were favorable for DAMO archaea. However, the effects of the periodic exposure and seawater immersion of the intertidal marsh sediments during tidal cycles on DAMO bacteria and DAMO archaea need to be further explored (Zhang et al., 2018).

Based on the stoichiometric-relationship of CH_4 and NO_2^- in the DAMO reaction (3:8), it was estimated that the nitrogen removal rates during the DAMO process ranged between 3.3 and 106.4 nmol N g^{-1} day^{-1} in the intertidal marsh sediments of the Yangtze Estuary. It was comparable to the nitrogen removal rate of the anaerobic ammonium oxidation (anammox) process in the intertidal marsh sediments of the Yangtze Estuary (22.6–158.6 nmol N g^{-1} day^{-1}), which was estimated to contribute 6.6 %–12.9% to the total nitrogen loss (the remainder being due to denitrification) in the study area (Fig. 5) (Hou et al., 2013). This result suggested that, in addition to playing an important role in the CH_4 sink, the DAMO process was a non-negligible pathway of nitrogen removal from the intertidal marshes.

Potential DAMO rates may be reflected by the abundance of DAMO microbes, so we expected significant relationships between them. In the present study, a significant correlation was only observed between the total DAMO potential and the abundance of the DAMO archaeal *mcrA* gene in winter ($P < 0.05$), suggesting that DAMO archaea might play a more important role in CH_4 oxidation than DAMO bacteria in winter. Sulfate-AOM has been suggested to be the main CH_4 removal pathway in marine habitats (Knittel and Boetius, 2009). However, in the Zhoushan intertidal zone, it was observed that the contribution of the DAMO process to CH_4 oxidation was greater than that of sulfate-AOM (Wang et al., 2019). The potential DAMO rate in the intertidal marsh sediments of the Yangtze Estuary (2.1–61.0 nmol $^{13}CO_2$ g^{-1} day^{-1}) was significantly higher than the sulfate-AOM rate (0–0.74 nmol $^{13}CO_2$ g^{-1} day^{-1}) detected in the Zhoushan intertidal zone (Wang et al., 2019), showing that the DAMO process was a crucial CH_4 sink in coastal ecosystems. Moreover, based on the standard Gibbs free energies (Table S1), denitrifying methanotrophs are energetically more favorable and may have an advantage in using CH_4 over the sulfate- and ferric iron-dependent methanotrophs in natural environments such as the intertidal marshes where NO_x^-, SO_4^{2-}, and Fe(III) coexist. However, further studies are still required to investigate and quantify the anaerobic oxidation of CH_4 driven by different electron acceptors in the intertidal wetlands.

5. Conclusions

DAMO bacteria and DAMO archaea coexisted and both were active in CH_4 oxidation in the intertidal flats. The DAMO archaeal *mcrA* gene had a higher diversity than the DAMO bacterial *pmoA* gene. The unvegetated low intertidal flat tended to be more favorable for the growth and activity of DAMO microorganisms, especially for DAMO archaea. Potential DAMO rates were significantly greater in summer than in winter, showing a higher activity of DAMO microbes in warm seasons. Overall, the nitrate-DAMO activity accounted for a higher proportion of total DAMO activity than nitrite-DAMO activity. In addition to playing an important role in the CH_4 sink, the DAMO process can also remove a substantial amount of reactive nitrogen from the coastal marshes. These results demonstrate the environmental significance of anaerobic CH_4 sinks coupled with denitrification in intertidal marsh sediments, and suggest that the DAMO bioprocess may play an important role in the coupled carbon and nitrogen transformations globally considering the worldwide distribution of intertidal wetlands.

Ethical approval

This article does not contain any studies with human participants or animals performed by any of the authors.

Declaration of competing interest

The authors declare that they have no conflict of interest.

Acknowledgments

This work was supported by the National Natural Science Foundation of China (Nos. 41601530, 41725002, 41671463, 41761144062, and 41730646); the Chinese National Key Programs for Fundamental Research and Development (No. 2016YFA0600904 and 2016YFE0133700); and the Yangtze Delta Estuarine Wetland Station, East China Normal University. Gene sequence data in this paper can be downloaded from GenBank with accession number MK888209-MK888681, and other data can be obtained by sending a written request to the corresponding author.

Appendix A. Supplementary data

Supplementary data to this article can be found online at https://doi.org/10.1016/j.marpolbul.2019.110681.

References

Barnes, R.O., Goldberg, E.D., 1976. Methane production and consumption in anoxic marine sediments. Geology 4, 297–300.
Bastviken, D., Tranvik, L.J., Downing, J.A., Crill, P.M., Enrich-Prast, A., 2011. Freshwater methane emissions offset the continental carbon sink. Science 331 50-50.
Costello, A.M., Lidstrom, M.E., California Inst Of Tech PU, 1999. Molecular characterization of functional and phylogenetic genes from natural populations of methanotrophs in lake sediments. Appl. Environ. Microbiol. 65, 5066–5074.
Dean, J.F., Middelburg, J.J., Röckmann, T., Aerts, R., Blauw, L.G., Egger, M., Jetten, M.S.M., de Jong, A.E.E., Meisel, O.H., Rasigraf, O., Slomp, C.P., In'T Zandt, M.H., Dolman, A.J., 2018. Methane feedbacks to the global climate system in a warmer world. Rev. Geophys. 56, 207–250.
Deutzmann, J.S., Schink, B., 2011. Anaerobic oxidation of methane in sediments of lake constance, an oligotrophic freshwater lake. Appl. Environ. Microbiol. 77, 4429–4436.
Ding, J., Ding, Z.W., Fu, L., Lu, Y.Z., Cheng, S.H., Zeng, R.J., 2015. New primers for detecting and quantifying denitrifying anaerobic methane oxidation archaea in different ecological niches. Appl. Microbiol. Biotechnol. 99, 9805–9812.
Ettwig, K.F., van Alen, T., van de Pas-Schoonen, K.T., Jetten, M.S.M., Strous, M., 2009. Enrichment and molecular detection of denitrifying methanotrophic bacteria of the NC10 phylum. Appl. Environ. Microbiol. 75, 3656–3662.
Ettwig, K.F., Butler, M.K., Paslier, D.L., Pelletier, E., Mangenot, S., Kuypers, M.M.M., Schreiber, F., Dutilh, B.E., Zedelius, J., de Beer, D., Gloerich, J., Wessels, H.J.C.T., van Alen, T., Luesken, F., Wu, M.L., van de Pas-Schoonen, K.T., Op Den Camp, H.J.M., Janssen-Megens, E.M., Francoijs, K., Stunnenberg, H., Weissenbach, J., Jetten, M.S.M., Strous, M., 2010. Nitrite-driven anaerobic methane oxidation by oxygenic bacteria. Nature 464, 543–548.
Ettwig, K.F., Zhu, B.L., Speth, D., Keltjens, J.T., Jetten, M.S.M., Kartal, B., 2016. Archaea catalyze iron-dependent anaerobic oxidation of methane. Proc. Natl. Acad. Sci. U.S.A. 113, 12792–12796.
Hales, B.A., Edwands, C., Ritchie, D.A., Hall, G., Pickup, R.W., Saunder, J.R., 1996. Isolation and identification of methanogen-specific DNA from blanket bog peat by PCR amplification and sequence analysis. Appl. Environ. Microbiol. 62, 668–675.
Haroon, M.F., Hu, S.H., Shi, Y., Imelfort, M., Keller, J., Hugenholtz, P., Yuan, Z.G., Tyson, G.W., 2013. Erratum: anaerobic oxidation of methane coupled to nitrate reduction in a novel archaeal lineage. Nature 500, 567–570.
Hinrichs, K.U., Hayes, J.M., Sylva, S.P., Brewer, P.G., DeLong, E.F., 1999. Methane-consuming archaebacteria in marine sediments. Nature 398, 802–805.
Holmes, A.J., Roslev, P., McDonald, I.R., Iversen, N., Henriksen, K., Murrell, J.C., 1999. Characterization of methanotrophic bacterial populations in soils showing atmospheric methane uptake. Appl. Environ. Microbiol. 65, 3312–3318.
Hou, L.J., Liu, M., Carini, S.A., Gardner, W.S., 2012. Transformation and fate of nitrate near the sediment–water interface of Copano Bay. Cont. Shelf Res. 35, 86–94.
Hou, L.J., Zheng, Y.L., Liu, M., Gong, J., Zhang, X.L., Yin, G.Y., You, L., 2013. Anaerobic ammonium oxidation (anammox) bacterial diversity, abundance, and activity in marsh sediments of the Yangtze Estuary. J. Geophys. Res. Biogeosci. 118, 1237–1246.
Hu, B.L., Shen, L.D., Lian, X., Zhu, Q., Liu, S., Huang, Q., He, Z.F., Geng, S., Cheng, D.Q., Lou, L.P., Xu, X.Y., Zheng, P., He, Y.F., 2014. Evidence for nitrite-dependent anaerobic methane oxidation as a previously overlooked microbial methane sink in wetlands. Proc. Natl. Acad. Sci. U.S.A. 111, 4495–4500.
Kintisch, E., 2013. Can coastal marshes rise above it all? Science 341, 480–481.
Knittel, K., Boetius, A., 2009. Anaerobic oxidation of methane: progress with an unknown process. Annu. Rev. Microbiol. 63, 311–334.
Kojima, H., Tsutsumi, M., Ishikawa, K., Iwata, T., Mußmann, M., Fukui, M., 2012. Distribution of putative denitrifying methane oxidizing bacteria in sediment of a freshwater lake, Lake Biwa. Syst. Appl. Microbiol. 35, 233–238.
Kumar, S., Stecher, G., Tamura, K., 2016. MEGA7: molecular evolutionary genetics analysis version 7.0 for bigger datasets. Mol. Biol. Evol. 33, 1870–1874.
Luesken, F.A., van Alen, T.A., van der Biezen, E., Frijters, C., Toonen, G., Kampman, C., Hendrickx, T.L.G., Zeeman, G., Temmink, H., Strous, M., Op Den Camp, H.J.M., Jetten, M.S.M., 2011a. Diversity and enrichment of nitrite-dependent anaerobic methane oxidizing bacteria from wastewater sludge. Appl. Microbiol. Biotechnol. 92, 845–854.
Luesken, F.A., Zhu, B.L., van Alen, T.A., Butler, M.K., Diaz, M.R., Song, B., Op Den Camp, H.J.M., Jetten, M.S.M., Ettwig, K.F., 2011b. *PmoA* primers for detection of anaerobic methanotrophs. Appl. Environ. Microbiol. 77, 3877–3880.
Lüke, C., Frenzel, P., 2011. Potential of *pmoA* amplicon pyrosequencing for methanotroph diversity studies. Appl. Environ. Microbiol. 77, 6305–6309.
Myhre, G., Shindell, D., Bréon, F.M., Collins, W., Fuglestvedt, J., Huang, J., Koch, D., Lamarque, J.F., Lee, D., Mendoza, B., Nakajima, T., Robock, A., Stephens, G., Takemura, T., Zhang, H., 2013. Anthropogenic and natural radiative forcing. In: Climate Change 2013: the Physical Science Basis. Contribution of Working Group I to the Fifth Assessment Report of the Intergovernmental Panel on Climate Change. Cambridge University Press, Cambridge.
Raghoebarsing, A.A., Pol, A., van de Pas-Schoonen, K.T., Smolders, A.J.P., Ettwig, K.F., Rijpstra, W.I.C., Schouten, S., Damsté, J.S.S., Op Den Camp, H.J.M., Jetten, M.S.M., Strous, M., 2006. A microbial consortium couples anaerobic methane oxidation to denitrification. Nature 440, 918–921.
Schloss, P.D., Westcott, S.L., Ryabin, T., Hall, J.R., Hartmann, M., Hollister, E.B., Lesniewski, R.A., Oakley, B.B., Parks, D.H., Robinson, C.J., Sahl, J.W., Stres, B., Thallinger, G.G., Van Horn, D.J., Weber, C.F., 2009. Introducing mothur: open-source, platform-independent, community-supported software for describing and comparing microbial communities. Appl. Environ. Microbiol. 75, 7537–7541.
Schwietzke, S., Sherwood, O.A., Bruhwiler, L.M.P., Miller, J.B., Etiope, G., Dlugokencky, E.J., Michel, S.E., Arling, V.A., Vaughn, B.H., White, J.W.C., Tans, P.P., 2016. Upward revision of global fossil fuel methane emissions based on isotope database. Nature 538, 88–91.
Segarra, K.E.A., Comerford, C., Slaughter, J., Joye, S.B., 2013. Impact of electron acceptor availability on the anaerobic oxidation of methane in coastal freshwater and brackish wetland sediments. Geochem. Cosmochim. Acta 115, 15–30.
Segarra, K.E.A., Schubotz, F., Samarkin, V., Yoshinaga, M.Y., Hinrichs, K., Joye, S.B., 2015. High rates of anaerobic methane oxidation in freshwater wetlands reduce potential atmospheric methane emissions. Nat. Commun. 6, 7477.
Shen, L.D., Liu, S., Huang, Q., Lian, X., He, Z.F., Geng, S., Jin, R.C., He, Y.F., Lou, L.P., Xu, X.Y., Zheng, P., Hu, B.L., 2014. Evidence for the cooccurrence of nitrite-dependent anaerobic ammonium and methane oxidation processes in a flooded paddy field. Appl. Environ. Microbiol. 80, 7611–7619.
Shen, L.D., Liu, S., He, Z.F., Lian, X., Huang, Q., He, Y.F., Lou, L.P., Xu, X.Y., Zheng, P., Hu, B.L., 2015. Depth-specific distribution and importance of nitrite-dependent anaerobic ammonium and methane-oxidising bacteria in an urban wetland. Soil Biol. Biochem. 83, 43–51.
Shen, L.D., Hu, B.L., Liu, S., Chai, X.P., He, Z.F., Ren, H.X., Liu, Y., Geng, S., Wang, W., Tang, J.L., Wang, Y.M., Lou, L.P., Xu, X.Y., Zheng, P., 2016. Anaerobic methane oxidation coupled to nitrite reduction can be a potential methane sink in coastal environments. Appl. Microbiol. Biotechnol. 100, 7171–7180.
Shen, L.D., Wu, H.S., Liu, X., Li, J., 2017. Cooccurrence and potential role of nitrite- and nitrate-dependent methanotrophs in freshwater marsh sediments. Water Res. 123, 162–172.
Shen, L.D., Ouyang, L., Zhu, Y.Z., Trimmer, M., 2019. Active pathways of anaerobic methane oxidation across contrasting riverbeds. ISME J. 13, 752–766.
Shi, Y., Wang, Z.Q., He, C.G., Zhang, X.Y., Sheng, L.X., Ren, X.D., 2017. Using ^{13}C isotopes to explore denitrification-dependent anaerobic methane oxidation in a paddy-

peatland. Sci. Rep. 7, 40848.
Strous, M., Jetten, M.S.M., 2004. Anaerobic oxidation of methane and ammonium. Annu. Rev. Microbiol. 58, 99–117.
Tamura, H., Goto, K., Yotsuyanagi, T., Nagayama, M., 1974. Spectrophotometric determination of iron(ii) with 1,10-phenanthroline in the presence of large amounts of iron(iii). Talanta 21, 314–318.
Vaksmaa, A., Jetten, M.S.M., Ettwig, K.F., Lüke, C., 2017a. *McrA* primers for the detection and quantification of the anaerobic archaeal methanotroph '*Candidatus* Methanoperedens nitroreducens'. Appl. Microbiol. Biotechnol. 101, 1631–1641.
Vaksmaa, A., Guerrero-Cruz, S., van Alen, T.A., Cremers, G., Ettwig, K.F., Lüke, C., Jetten, M.S.M., 2017b. Enrichment of anaerobic nitrate-dependent methanotrophic '*Candidatus* Methanoperedens nitroreducens' archaea from an Italian paddy field soil. Appl. Microbiol. Biotechnol. 101, 7075–7084.
Wang, J.Q., Cai, C.Y., Li, Y.F., Hua, M.L., Wang, J.R., Yang, H.R., Zheng, P., Hu, B.L., 2019. Denitrifying anaerobic methane oxidation: a previously overlooked methane sink in intertidal zone. Environ. Sci. Technol. 53, 203–212.
Wang, S.H., Wu, Q., Lei, T., Liang, P., Huang, X., 2016. Enrichment of denitrifying methanotrophic bacteria from Taihu sediments by a membrane biofilm bioreactor at ambient temperature. Environ. Sci. Pollut. Res. 23, 5627–5634.
Wang, Y., Zhu, G.B., Harhangi, H.R., Zhu, B.L., Jetten, M.S.M., Yin, C.Q., Camp, H.J.M.O., 2012. Co-occurrence and distribution of nitrite-dependent anaerobic ammonium and methane-oxidizing bacteria in a paddy soil. FEMS Microbiol. Lett. 336, 79–88.
Weber, H.S., Habicht, K.S., Thamdrup, B., 2017. Anaerobic methanotrophic archaea of the ANME-2d cluster are active in a low-sulfate, iron-rich freshwater sediment. Front. Microbiol. 8, 619.
Winkel, M., Mitzscherling, J., Overduin, P.P., Horn, F., Winterfeld, M., Rijkers, R., Grigoriev, M.N., Knoblauch, C., Mangelsdorf, K., Wagner, D., Liebner, S., 2018. Anaerobic methanotrophic communities thrive in deep submarine permafrost. Sci. Rep. 8, 1291.
Wu, M.L., Ettwig, K.F., Jetten, M.S.M., Strous, M., Keltjens, J.T., Niftrik, L.V., 2011. A new intra-aerobic metabolism in the nitrite-dependent anaerobic methane-oxidizing bacterium *Candidatus* 'Methylomirabilis oxyfera'. Biochem. Soc. Trans. 39, 243–248.
Xu, H.J., Wang, X.H., Li, H., Yao, H.Y., Su, J.Q., Zhu, Y.G., 2014. Biochar impacts soil microbial community composition and nitrogen cycling in an acidic soil planted with rape. Environ. Sci. Technol. 48, 9391–9399.
Xu, S., Lu, W.J., Mustafa, M.F., Caicedo, L.M., Guo, H.W., Fu, X.D., Wang, H.T., 2017. Co-existence of anaerobic ammonium oxidation bacteria and denitrifying anaerobic methane oxidation bacteria in sewage sludge: community diversity and seasonal dynamics. Microb. Ecol. 74, 832–840.
Yang, J., Jiang, H.C., Wu, G., Hou, W.G., Sun, Y.J., Lai, Z.P., Dong, H.L., 2012. Co-occurrence of nitrite-dependent anaerobic methane oxidizing and anaerobic ammonia oxidizing bacteria in two Qinghai-Tibetan saline lakes. Front. Earth Sci. PRC 6, 383–391.
Zehnder, A.J., Brock, T.D., 1979. Methane formation and methane oxidation by methanogenic bacteria. J. Bacteriol. 137, 420–432.
Zhang, M.P., Luo, Y., Lin, L.A., Lin, X.L., Hetharua, B., Zhao, W.J., Zhou, M.K., Zhan, Q., Xu, H., Zheng, T.L., Tian, Y., 2018. Molecular and stable isotopic evidence for the occurrence of nitrite-dependent anaerobic methane-oxidizing bacteria in the mangrove sediment of Zhangjiang Estuary, China. Appl. Microbiol. Biotechnol. 102, 2441–2454.
Zheng, Y.L., Hou, L.J., Liu, M., Yin, G.Y., Gao, J., Jiang, X.F., Lin, X.B., Li, X.F., Yu, C.D., Wang, R., 2016. Community composition and activity of anaerobic ammonium oxidation bacteria in the rhizosphere of salt-marsh grass *Spartina alterniflora*. Appl. Microbiol. Biotechnol. 100, 8203–8212.
Zhou, L.L., Wang, Y., Long, X.E., Guo, J.H., Zhu, G.B., 2014. High abundance and diversity of nitrite-dependent anaerobic methane-oxidizing bacteria in a paddy field profile. FEMS Microbiol. Lett. 360, 33–41.
Zhu, G.B., Zhou, L.L., Wang, Y., Wang, S.Y., Guo, J.H., Long, X.E., Sun, X.B., Jiang, B., Hou, Q.Y., Jetten, M.S.M., Yin, C.Q., 2015. Biogeographical distribution of denitrifying anaerobic methane oxidizing bacteria in Chinese wetland ecosystems. Environ. Microbiol. Rep. 7, 128–138.